Clamping Strategy for Single-Layer Wire Arc Additive Manufacturing Using Gas Metal Arc Welding of the AA6061 Substrate and ER5356 Filler

Afrizal Riyantono[1], Agus Sifa[1], Faza Khoirina[1], Agus Sentana[1], Ario Sunar Baskoro[1]*, Gandjar Kiswanto[1]
[1]Department of Mechanical Engineering, Faculty of Engineering, Universitas Indonesia, Depok, 16424, Indonesia
*Corresponding author's : ario@eng.ui.ac.id

Abstract. Wire Arc Additive Manufacturing is a Direct Energy Deposition process that uses an electric arc as the heat source to melt metal wire layer by layer. WAAM-based additive manufacturing presents one of its main challenges: material deformation caused by thermal effects during the welding process. In this study, the materials used were AA6061 as the substrate and ER5356 as the filler. The novelty of this research lies in its analysis of clamping configurations as a primary variable for controlling distortion during the WAAM of aluminum. This approach yields significant benefits in cost reduction, product quality enhancement, and time efficiency. This research aims to determine the most effective method for evaluating, both experimentally and numerically, the effect of different substrate clamping strategies on distortion and residual stress in the WAAM process. The experimental results show that the maximum temperature recorded by the thermal gun reached 828°C in Strategy 2. In contrast, the simulations showed a peak temperature of 912°C. The simulation results also indicated that the highest Von Mises stress occurred in strategy 4 is the one with the highest residual stress among the others, reaching 59.62 MPa. Both the experimental and simulation results for Strategy 8 showed the smallest deflection in the substrate area, with a maximum difference of only 0.20 mm in the experiment and 0.13 mm in the simulation at certain points. The low deflection in Strategy 8 suggests that the number and positioning of clamps during the WAAM process have a significant impact on reducing substrate deflection.

Keywords: AA6061; Clamping; ER5356; GMAW; WAAM.

1 Introduction

Wire Arc Additive Manufacturing (WAAM) is a Direct Energy Deposition (DED) additive manufacturing process that uses an electric arc as a heat source to melt metal wire layer by layer [1]. One common approach involves the use of Gas Metal Arc Welding (GMAW) technology with argon shielding gas. A key advantage of the WAAM process is its potential to reduce process time and the ability to manufacture complex geometries that are difficult or impossible to process with conventional machining processes like milling or lathe. WAAM utilizes automated robotic

S. C. Asih et al. (eds.), *Proceedings of the 19th International Conference on Quality in Research (QiR 2025)*, Advances in Engineering Research 303,
https://doi.org/10.2991/978-94-6239-717-0_16

movement technologies, such as Computer Numerical Control (CNC) machines operating on three axes, combined with welding technology to produce three-dimensional components [2].

In its operation, WAAM introduces one of the major challenges in additive manufacturing: material deformation caused by thermal effects during welding. WAAM builds up metal components in stages using electric arc welding to deposit successive layers of weld metal. This process results in repeated thermal cycling, which can cause deformation due to volumetric shrinkage, thermal distortion, and residual stress. Thermal deformation in WAAM occurs when there is an uneven thermal distribution during the deposition of the molten metal.

In this study, the materials used were AA6061 as the substrate and ER5356 as the filler metal. According to J.R. Davis [3], aluminum possesses a unique combination of properties such as low density, corrosion resistance, and high thermal conductivity. Due to its high thermal conductivity, aluminum is a particularly interesting material for research in WAAM. The rapid heat dissipation enabled by this property influences the deposition process and allows further investigation into the distortion and deformation risks.

Previous studies by Kozamernik [4] and Sun [5] have focused on thermal parameters such as heat input, travel speed, and interlayer cooling methods. Several simulation-based studies on aluminum WAAM have also been conducted using software such as Abaqus. For example, Han [6] demonstrated that altering the torch path pattern can reduce distortion in the aluminum WAAM processes. However, despite improvements in the path strategies, residual stress and deformation remain difficult to control and generally remain high. Rameez Israr [7] investigated various clamping configurations on steel grade 09L and found that different fixation strategies, especially transverse and corner clamps, significantly influenced residual stress and distortion. This study was conducted through numerical simulation using LS-DYNA without experimental validation. Other complex WAAM simulations have also been explored; for example, Zhao [8] used the Finite Element Method (FEM) to analyze the reinforcement processes on half-cylinder WAAM components.

Building upon these previous studies, the present research aims to determine the most effective evaluation method—both experimental and simulation-based—for assessing the impact of different substrate clamping strategies on distortion and residual stress in aluminium alloys WAAM using AA6061 as the substrate and ER5356 as the filler metal. In industry, operators usually rely on intuition or trial and error in practice. This paper moves away from that approach by using data, showing that Strategy 8 is the most effective for reducing deformation. Another important point is that by implementing the best clamping strategy from the beginning, industry can reduce product failures caused by deformation and avoid rework, leading to greater efficiency in both time and production costs. Using a FEM approach with Abaqus software, this study performs a three-dimensional thermal analysis incorporating layer-by-layer element activation and the Goldak double-ellipsoid heat source model. This research seeks to fill existing gaps in the literature that have yet to be fully explored and aims to contribute practical insights toward the development of more effective and efficient clamping designs for aluminum WAAM processes.

2 Materials and Methods

This section presents a comprehensive overview of the experimental approach used to directly evaluate the effects of the substrate clamping strategies, as well as the finite element-based numerical simulation of thermal distortion and residual stress in the WAAM process. The first part describes the materials used in the study and the design of the specimens to be analyzed. The second part outlines the research methodology employed in the experimental WAAM process using GMAW. The third part explains the simulation methods applied in modelling the WAAM welding process.

2.1 Materials

This study utilizes AA6061 alloy as the substrate, with dimensions of 250 mm × 60 mm × 6 mm, and ER5356 metal filler in the form of wire with a diameter of 1.2 mm. The weld deposit geometry is modeled with a length of 200 mm and consists of a single vertical layer. The thermophysical properties of both materials were obtained from Summers [9] for AA6061 and Wieczorowski [10] for ER5356.

Table 1 *Material Properties*

Material Properties	AA6061[9]	ER5356[10]
Thermal Conductivity, k (W/m.K)	170	121.8
Density, ρ (kg/m^3)	2690	2640
Modulus Young E(GPa)	69.5	70
Thermal Expansion, α° (C^{-1})	2.79E-05	2.20E-05
Specific Heat, c (J/kg.K)	900	900
Poissons Ratio, μ	0.33	0.33

According to Tawfik [11], the material properties of aluminum in the filler metal can exhibit improvements compared to the substrate, particularly in terms of tensile strength and hardness. All properties listed in Table 1 were defined as material parameters and implemented into Abaqus Simulia using a user-defined material (UMAT) — allows users to define their own material models that are not included in the software's default library.

2.2 Experimental Methods

Figure 1 shows the experimental apparatus. The WAAM process in this study was carried out using a GMAW machine integrated with a CNC system, which was modified for additive manufacturing applications. The machine was controlled using the UGS Platform application, which provides control over the current, voltage, and torch travel speed. Using these parameters, the heat input can be calculated based based on standard welding formulas [12,13]:

$$Q = \frac{\eta \times I \times V}{v} \quad (1)$$

Where :
Q = Heat input per unit length, (J/mm)
η = Thermal efficiency process
I = Electric current, Ampere (A)
V = Electric voltage, Volt (V)
v = Torch movement speed, (mm/s)

The surface of the substrate was cleaned with acetone before welding to prevent contamination and ensure optimal wetting of the filler material. The torch was moved at a constant feed rate of 140 mm/min, and the process was carried out along the Y-axis in the horizontal direction. ER5356 filler wire with a diameter of 1.2 mm was used along, with an AA6061 aluminum substrate that had been cleaned before processing. The Contact Tip to Workpiece Distance (CTWD) was set to 20 mm [14–16].

Table 2 *Parameters of the welding process*

Parameters	Value
Current	90 A
Voltage	13.3 V
Welding Feed Rate	140 mm/min (2.33 mm/s)
Shielding Gas	Argon (15 L/min)

The following calculation was used to determine the amount of heat applied per unit length during the WAAM process. By knowing the heat input from this calculation, both the experimental and simulation processes can be conducted more effectively to reflect realistic thermal conditions. In this study, as shown in Table 2, the following welding parameters were used: current of 90 A, voltage of 13.4 V, thermal efficiency of 0.8, and a travel speed of 2.33 mm/s, resulting in a calculated heat input of 459 J/mm.

$$Q = \frac{0.8 \times 90 \times 13.3}{2.33} = 410.9\, J/mm$$

As shown in Figure 1, the temperature measurements were carried out using a Krisbow infrared thermometer to determine the maximum temperature, calibrated with an aluminum surface emissivity of 0.2[17]. The cooling process occurred under ambient conditions without the aid of fans or force cooling. The ambient temperature during the experiment was approximately 25°C (298.15 K).

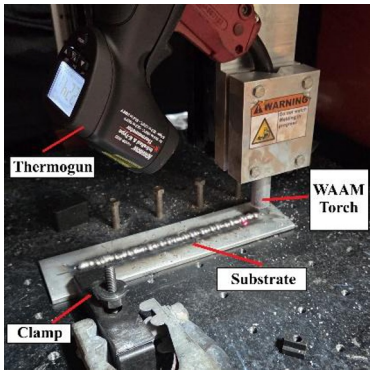

Figure 1 Experimental apparatus

The WAAM process used GMAW, which relies on fusion to melt the material. The heat distribution that occurs during this process can be analyzed using the Goldak Double Ellipsoid heat source model [18–21];

The Goldak Double Ellipsoid model for the heat distribution in the front region is defined as

$$qf(x,y,z,t) = \frac{6\sqrt{3}f\,fq}{afbc\pi\sqrt{\pi}} exp - (\frac{3x^2}{af^2} + \frac{3y^2}{b^2} + \frac{z^2}{c^2}) \quad (2)$$

The Goldak Double Ellipsoid model for the heat distribution in the rear region is defined as

$$qf(x,y,z,t) = \frac{6\sqrt{3}f\,rq}{afbc\pi\sqrt{\pi}} exp - (\frac{3x^2}{ar^2} + \frac{3y^2}{b^2} + \frac{z^2}{c^2}) \quad (3)$$

$$qf(x,y,z) = qf(x,y,z)\ for\ x \geq 0\ (front\ ellipsoid)$$

$$qf(x,y,z) = qr(x,y,z)\ for\ x \leq 0\ (rear\ ellipsoid)$$

where:

Q = total energy input (W)

$$Q = \mu VI \quad (4)$$

a,b,c = Parameters that define the shape of the heat distribution

x,y,z = Coordinates in the local coordinate system of the heat source

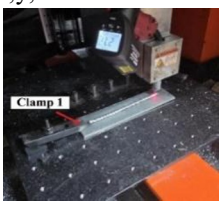

Strategy 1

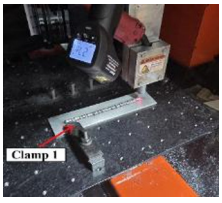

Strategy 2

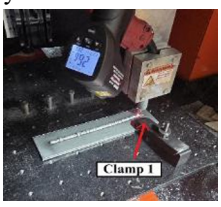

Strategy 3

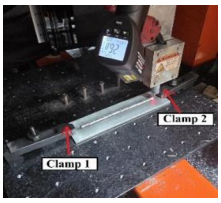

Strategy 4

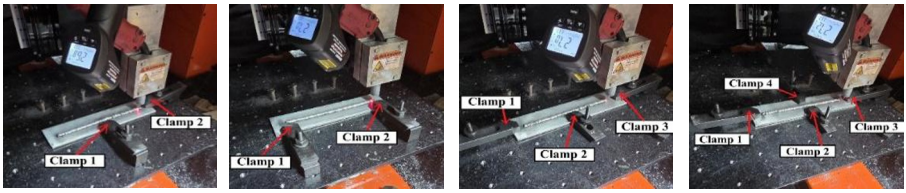

Strategy 5 Strategy 6 Strategy 7 Strategy 8

Figure 2 Experiment of WAAM Clamping

The double ellipsoid heat source from Goldak's equation closely approximates the actual welding conditions, which model the heat flux distribution of the WAAM process [22]. The double ellipsoid heat source model captures the asymmetric condition of the heat distribution during welding and consists of two condition regions, the front and rear [23].

Figure 2 shows the position of WAAM clamping. Eight strategies were modeled based on common industrial practices, such as clamping the workpiece at its end. These combinations were designed to observe the phenomena that occur when using one, two, or three clamps, allowing for a comparison between different levels of fixation. After the WAAM process is completed, the specimen is allowed to cool naturally to an ambient temperature (25°C). The heating and cooling cycles during WAAM result in a non-uniform thermal stress distribution, leading to permanent deformation in the aluminum substrate. As shown in Fig. 3, the thermally induced deformation profile, typically characterized by bending, was measured using a vernier caliper.

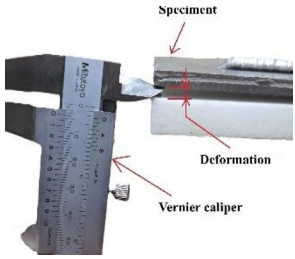

Figure 3 Measuring deformation using a vernier caliper

2.3 Simulation Methods

Abaqus Simulia was used for this simulation with a coupled temperature–displacement procedure. Activated sequentially using the birth element technique, the ER5356 filler was divided into 40 segments, each 5 mm in length. The coefficient of thermal expansion, Young's modulus, heat capacity, density, and thermal conductivity were defined as listed in 1 as the material properties. The FEM is an effective approach for predicting distortion caused by thermal residual stress, as demonstrated by Ying Ying Di [24], who investigated process optimization prior to the WAAM process for stainless stell.

Figure 4 Fixation strategy

Boundary conditions and interactions were defined as Montevecchi [25] adopted with solution of isostatic to eliminate distortion. In this study, the ends of the substrate were fixed to prevent any total free movement, as shown in Fig. 2 for experiment and Fig. 4 for simulation. Thermal losses were also defined using heat convection, implemented via a film condition applied to the top surfaces of both the filler and the substrate, with a convection coefficient of h = 20 W/m²·K and ambient temperature of 25°C. In addition, radiation was applied to the top surface with an emissivity of 0.2 and a Stefan–Boltzmann constant of 5.67×10^{-8} W/m²·K⁴[26].

The thermal load input was derived from the calculations, resulting in a total heat input of 410.9 J/mm. A hex element is used for this simulation with the 'as-is' technique, using a 1 mm mesh in the filler and a 2 mm mesh in the substrate. For each 5 mm segment, this was distributed across 225 nodes, giving an average heat input of approximately 4.29 W/node, which was applied as a concentrated heat flux (coupled temperature–displacement analysis). The simulation was run with 40 steps representing one layer, where each step corresponds to 2.14 seconds, based on the calculation of the segment length divided by the torch travel speed. Temperature data were collected from several points above the filler after the WAAM process, as shown in Fig. 5(a). Deformation and residual stress data were collected from 26 points, as shown in Fig. 5(b).

$$\text{Step Time per Cell} = \frac{\text{Cell length}}{\text{Torch travel speed}} = \frac{5\ mm}{2.33\ mm/s} = 2.14\ s$$

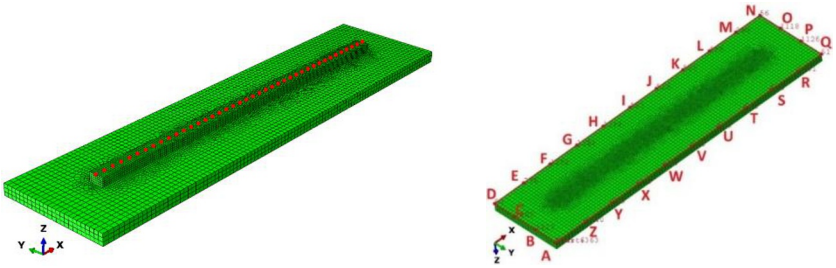

Figure 5 (a) Node point for capturing the maximum temperature; (b) Data extraction point for the deformation and residual stress

3 Result

3.1 Experimental and Simulation Temperature Results

Temperature measurements during the WAAM process were carried out using an infrared thermometer. In practice, the thermal gun was positioned in such a way that it moved in the same direction as the welding torch. To ensure that measurements near the heat source are accurate, this scheme observes dynamic temperature changes following the position and time during heat movement [27].

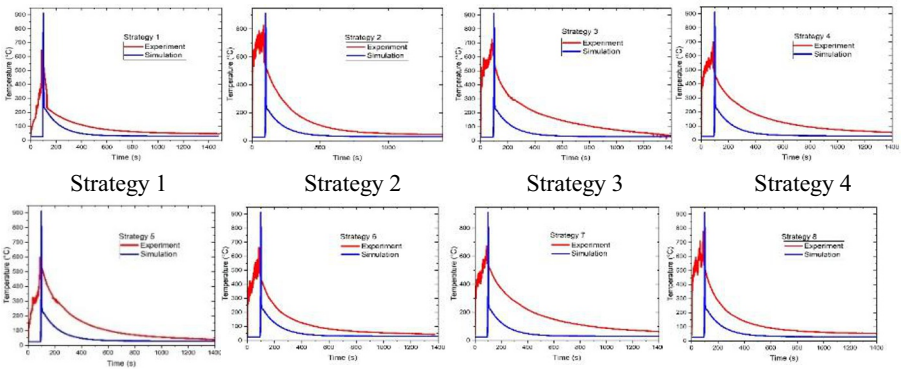

Figure 6 Temperature result from experiment and simulation

Maximum temperature was measured using a thermogun and resulted in peak temperature. As shown in Fig. 6, from the experiment in Strategy 1 reached 647°C, Strategy 2 reached 828°C, Strategy 3 reached 728°C, Strategy 4 reached 698°C, Strategy 5 reached 597°C, Strategy 6 reached 662°C, Strategy 7 reached 676°C, and Strategy 8 reached 778°C. From the experimental welding process, this value is

significantly meaningful for validating the result of the simulation and represents the maximum temperature from heat accumulation.

The thermal output from the WAAM simulation showed temperature distribution based on the concentrated heat flux approach as defined by Eq. 1. Figure 7 shows the WAAM temperature distribution in Celius. The heat source was modeled as a concentrated heat flux applied progressively to the active elements using the element birth technique, in accordance with the torch movement speed used in the experiment. The maximum temperature across all strategies was identical due to the use of consistent input parameters and ideal conditions in each strategy. The model applied a concentrated heat flux with a configuration of 40 segments per layer and a torch travel speed of 2.33 mm/s, matching the experimental setup. The simulation results indicated a peak temperature of 912°C, observed at three nodes before the final node as shown in Fig. 5 (a).

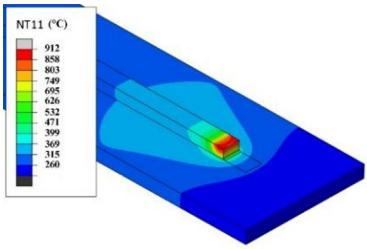

Figure 7 WAAM temperature distribution

3.2 Residual Stress Result

The WAAM simulation of aluminum showed residual stresses caused by the accumulation of heat and subsequent cooling during the process. The peak von Mises stress was observed near the surface and in the transition zones between the layers. Sun [28] studied the longitudinal stress, as more layers are added, von mises stress from aluminum resulting from the WAAM process is influenced by the substrate deformation and deposition height.

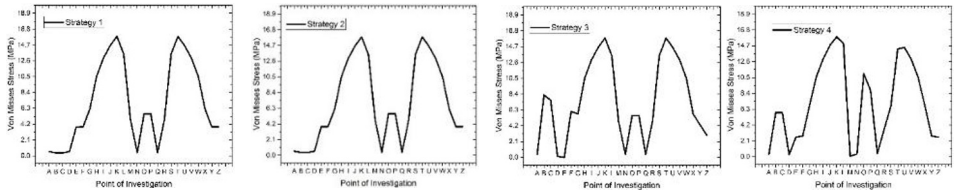

Strategy 1 Strategy 2 Strategy 3 Strategy 4

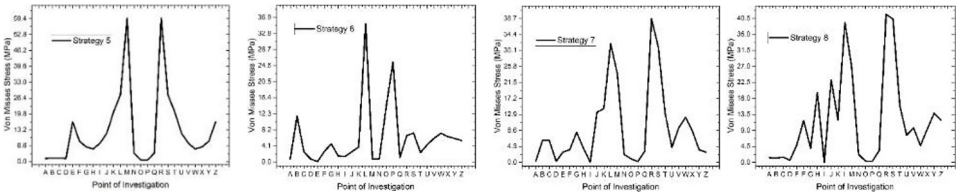

Strategy 5 Strategy 6 Strategy 7 Strategy 8

Figure 8 Von misses stress

As shown in Fig. 8, strategy 1, 2, and 3 show very similar results with two points indicating peaks of residual stress at 15.84 MPa at point J and T. Strategy 4 is the one with the highest residual stress among the others, reaching 59.62 MPa at point M and R. Strategy 5 shows high residual stress at point L with a value of 35.27 MPa. Strategy 6 shows high residual stress at point R with a value of 38.61 MPa. Strategy 7 shows high residual stress at point R with a value of 41.58 MPa. Strategy 8 shows high residual stress at two points, L and S, with a value of 46.31 MPa. Strategy 8 provides the most complete fixation compared to the other strategies, which effectively prevent deformation or bending. However, this complete fixation restricts the material prevention during the cooling period, resulting in high residual stress within the material. Challenges in additive manufacturing processes, as illustrated in the study by Rodrigues [29], often center on uneven thermal management, sharp temperature gradients between a hot new layer and the cooler substrate beneath it can lead to micro-defects and high internal stresses in the final component. Heat and cold cycles occurred from the WAAM process, resulting in a high level of stress. To control distortion, simulation-based modeling becomes essential, as demonstrated in the study by Grilli [30] which visualized von Mises stress development throughout the WAAM process.

3.3 Deformation Result

Deformation on the WAAM substrate is visually observed as bending or dimensional deviation, which represents the macroscopic result of the complex heat accumulation and residual stress.

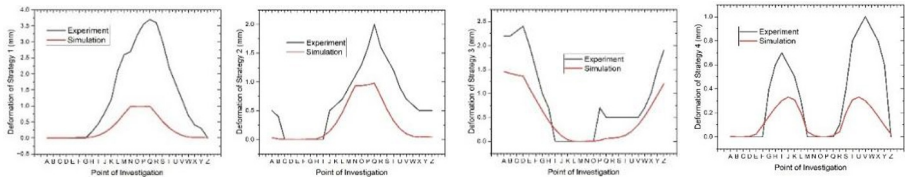

Strategy 1 Strategy 2 Strategy 3 Strategy 4

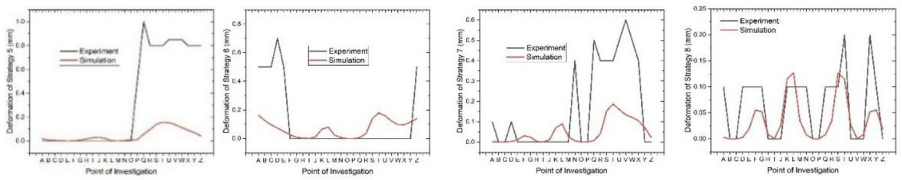

Figure 9 Deformation result of the experiment and simulation

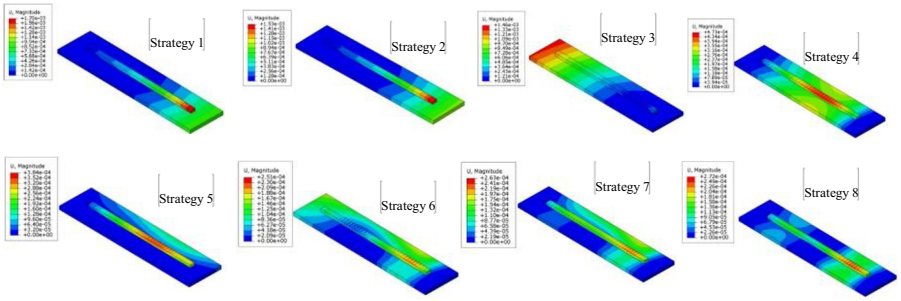

Figure 10 Deformation result in meters

As shown in Fig. 9 and Fig. 10, strategy 8 exhibited the smallest deflection in the substrate area, with a maximum deviation of only 0.20 mm in the experiment and 0.13 mm in the simulation at several points. Strategy 1 reached peak deformation of 3.5 mm in the experiment at point Q, and 0.98 mm in the simulation at points N and Q. Strategy 2 reached a peak deformation of 2 mm in the experiment at point Q, and 1 mm in the simulation at point Q. Strategy 3 reached a peak deformation of 2.45 mm in the experiment at point D, and 1.45 mm in the simulation at point A. Strategy 4 reached a peak deformation of 1 mm in the experiment at point V, and 0.3 mm in the simulation at points J and U. Strategy 5 reached a peak deformation of 1 mm in the experiment at point Q, and 0.15 mm in the simulation at point T. Strategy 6 reached a peak deformation of 0.7 mm in the experiment at point D, and 0.2 mm in the simulation at point T. Strategy 7 reached a peak deformation of 0.6 mm in the experiment at point V, and 0.18 mm in the simulation at point T. Strategy 8 reached a peak deformation of 0.2 mm in the experiment at points T and X, and 0.13 mm in the simulation at points S and L. This reduced deflection indicates that the increased number of clamps during the WAAM process had a significant effect in minimizing the substrate deformation. The level of distortion observed in the experiment aligns with the mechanism of uneven thermal accumulation described by Wu [31] as a primary cause of deformation in the WAAM process.

In general, the results from the experiment and the simulation show a consistent pattern and trend of deformation, despite the difference in values between the experiment and simulation. Basic assumptions in the simulation, simplification approaches, and experimental schemes not being close to ideal conditions result in differences in the results. Understanding the general trend and behavior observed

during the WAAM process in both the simulation and the experiment is the goal of this validation.

4 Discussion

The comparison between the experimental and simulation results demonstrates a consistent trend and pattern in both the temperature distribution and deformation occurring in the substrate. The maximum temperature recorded in the experiment reached 828°C, while the simulation produced a peak of 912°C, the difference between those two values is 9.66%. This indicates that Equation 1 is sufficiently representative in modeling thermal behavior during the WAAM process. A deviation of 9.66% was considered acceptable. Factors that cause experimental uncertainty include thermogun positioning and room temperature fluctuations due to weather. In contrast, simulations assume all conditions are ideal and uniform.

In general, the residual stress results provide insight into the magnitude of stress occurring in the substrate area. Specifically, the concentration of stress and deformation indicates that material cooling leads to shrinkage in the layers, resulting in residual stress and permanent deformation. The slightly higher experimental deformation compared to the simulation results is due to idealized assumptions in the model and inherent uncertainties. Experimental sources of uncertainty include ambient temperature variations and measurement tool tolerances, while simulation uncertainties stem from mesh discretization and idealized boundary conditions.

This paper offers a methodology that combines experiments and simulations, which can be extended to evaluate clamping strategies for curved or complex-shaped parts. Although the geometry used in this paper is general, the optimal strategy depends on the size and complexity of the geometry. For products larger than those in this study, adjustments to the clamping are required. This paper can be used as a reference for simulating clamping strategies.

Overall, the findings of this study support and expand the current understanding of the WAAM process, particularly for aluminum materials. More specifically, it contributes to the understanding of effective clamping strategies that can be applied during aluminum WAAM processes. These results provide a meaningful contribution toward more efficient process development while remaining consistent with experimental conditions. This research is relevant for single-layer deposition because welding is applied directly to the substrate material, making heat accumulation and interaction highly significant. In multilayer cases, such as when a second layer is deposited on the first, the substrate becomes less critical. Besides these results, Williams [32] studied that heat distribution from the electric arc causes high residual stress, but symmetrical strategies from deposition reduce distortion from the substrate. Yang [33] studied that heat input control and interlayer cooling are crucial for reducing thermal accumulation and reducing residual stress and cracks from the aluminum WAAM process. Sarikaya [34] studied that heat input control and interlayer cooling are crucial for reducing thermal accumulation and reducing residual stress and cracks from the aluminum WAAM process. Elangovan [35] studied that cooling mechanical processes can

significantly reduce residual stress, suggesting cooling strategies in the future. Future studies may further investigate distortion control, including more advanced cooling strategies, welding parameter variations, and interlayer techniques.

5 Conclusion

In this study, the experimental and simulation results were compared in terms of temperature and deformation caused by heat accumulation. The following conclusions can be drawn:

1. The relationship between deformation and residual stress is strongly correlated with the WAAM process. Deformation arises due to non-uniform heating and cooling, which is a direct result of the residual stress accumulation during the WAAM process.
2. The simulation model successfully captured the main trends of dimensional changes in the substrate, indicating that this approach can be used to predict distortion and control deformation in WAAM manufacturing.
3. The simulation approach using the heat flux applied to the nodes and the controlled ambient temperature produced results that closely matched experimental conditions.
4. Strategy 4 is the one with the highest residual stress among the others, reaching 59.62 MPa.
5. Strategy 8 is the best strategy based on the results of this paper because it results in the smallest deflection of the substrate, with a peak deformation of just 0.20 mm in the experiment and 0.13 mm in the simulation at several points. This strategy showed a peak temperature of 778°C in the experiment, while the simulation showed 912°C. The peak von mises stress from strategy 8 is 46.31 MPa.

Acknowledgments. This research is supported by the Fundamental Research Regular Year 2024 Program from the Ministry of Higher Education, Science, and Technology, Republic of Indonesia, with contract number: No. NKB-924/UN2.RST/HKP.05.00/2024. The authors would also like to express their sincere gratitude to Badan Riset dan Inovasi Nasional (BRIN) for its valuable contribution in providing the Abaqus software, which greatly supported the simulation requirements of this research.

Disclosure of Interests. The authors declare that they have no conflict of interest.

References

[1] Li Y, Su C, Zhu J. Comprehensive review of wire arc additive manufacturing: Hardware system, physical process, monitoring, property characterization, application and future prospects. Results in Engineering 2022;13. https://doi.org/10.1016/j.rineng.2021.100330.

[2] Guo C, Lin Q, Hu R, Wu S. Research Progress and Application Scenarios of Wire + Arc Additive Manufacturing: From Process Control to Performance Evaluation. Micromachines (Basel) 2025;16:749. https://doi.org/10.3390/mi16070749.

[3] J.R. Davis. Aluminum and Aluminum Alloys Introduction and Overview 2001. https://doi.org/10.1361/autb2001p351.
[4] Kozamernik N, Drago Bračun &, Klobčar D. WAAM system with interpass temperature control and forced cooling for near-net-shape printing of small metal components n.d. https://doi.org/10.1007/s00170-020-05958-8/Published.
[5] Sun G, Sun X, Zhao X, Chen C. Effect of interlayer rapid cooling on the microstructure and properties of aluminum alloys produced by wire arc additive manufacturing. Manuf Lett 2024;40:70–4. https://doi.org/10.1016/j.mfglet.2024.03.001.
[6] Han Y. A Finite Element Study of Wire Arc Additive Manufacturing of Aluminum Alloy. Applied Sciences (Switzerland) 2024;14. https://doi.org/10.3390/app14020810.
[7] Israr R, Buhl J, Bambach M. Numerical analysis of different fixation strategies in direct energy deposition processes. Procedia Manuf, vol. 47, Elsevier B.V.; 2020, p. 1184–9. https://doi.org/10.1016/j.promfg.2020.04.145.
[8] Zhao XF, Zapata A, Bernauer C, Baehr S, Zaeh MF. Simulation of Wire Arc Additive Manufacturing in the Reinforcement of a Half-Cylinder Shell Geometry. Materials 2023;16. https://doi.org/10.3390/ma16134568.
[9] Summers PT, Chen Y, Rippe CM, Allen B, Mouritz AP, Case SW, et al. Overview of aluminum alloy mechanical properties during and after fires. Fire Sci Rev 2015;4. https://doi.org/10.1186/s40038-015-0007-5.
[10] Wieczorowski M, Pereira A, Carou D, Gapinski B, Ramírez I. Characterization of 5356 Aluminum Walls Produced by Wire Arc Additive Manufacturing (WAAM). Materials 2023;16. https://doi.org/10.3390/ma16072570.
[11] Tawfik MM, Nemat-Alla MM, Dewidar MM. Enhancing the properties of aluminum alloys fabricated using wire + arc additive manufacturing technique - A review. Journal of Materials Research and Technology 2021;13:754–68. https://doi.org/10.1016/j.jmrt.2021.04.076.
[12] Zeng J, Nie W, Li X. The influence of heat input on the surface quality of wire and arc additive manufacturing. Applied Sciences (Switzerland) 2021;11. https://doi.org/10.3390/app112110201.
[13] Ríos S, Colegrove PA, Martina F, Williams SW. Analytical process model for wire + arc additive manufacturing. Addit Manuf 2018;21:651–7. https://doi.org/10.1016/j.addma.2018.04.003.
[14] Henckell P, Gierth M, Ali Y, Reimann J, Bergmann JP. Reduction of energy input in wire arc additive manufacturing (WAAM) with gas metal arc welding (GMAW). Materials 2020;13. https://doi.org/10.3390/ma13112491.
[15] Thien A, Saldana C, Kurfess T. The Effect of WAAM Process Parameters on Process Conditions and Production Metrics in the Fabrication of Single-pass Multi-layer Wall Artifacts. n.d.
[16] Fajrin A, Giat L, Putra J, Rezkian B. Perbandingan Weld Bead terhadap Contact Tip to Work Distance (CTWD) pada Mesin Welding Tractor GMAW. vol. 12. 2021.
[17] Transmetra. Table of emissivity of various surfaces for infrared thermometry. n.d.
[18] Cheng J, Huo Y, Fernandez-Zelaia P, Hu X, Li M, Sun X. A Gaussian Process-Based extended Goldak heat source model for finite element simulation of laser powder bed fusion additive manufacturing process. Comput Mater Sci 2024;244. https://doi.org/10.1016/j.commatsci.2024.113185.
[19] Liu X, Jiang L, Cheng G, Liu J, Xu B, Jin R. Residual Stress Distribution and Fatigue Behavior of Combined Bolted–Welded Joints. Buildings 2025;15. https://doi.org/10.3390/buildings15060910.

[20] Schauenberg AS, Rodríguez RQ, Almeida DT, Zanon JE, Cunha E, Lopes APO, et al. Evaluating thermal gradient in GMAW welding process with a novel heat source model: Numerical and experimental approach. Eng Struct 2024;318. https://doi.org/10.1016/j.engstruct.2024.118724.

[21] Moslemi N, Gohari S, Abdi B, Sudin I, Ghandvar H, Redzuan N, et al. A novel systematic numerical approach on determination of heat source parameters in welding process. Journal of Materials Research and Technology 2022;18:4427–44. https://doi.org/10.1016/j.jmrt.2022.04.039.

[22] Sampaio RFV, Pragana JPM, Bragança IMF, Silva CMA, Nielsen C V., Martins PAF. Modelling of wire-arc additive manufacturing – A review. Advances in Industrial and Manufacturing Engineering 2023;6. https://doi.org/10.1016/j.aime.2023.100121.

[23] Kim Y, Kim J, Park H, Hong S, Pyo C, Park G. An Improved Method for Deriving the Heat Source Model for FCAW of 9% Nickel Steel for Cryogenic Tanks. Materials 2023;16. https://doi.org/10.3390/ma16206647.

[24] Di YY, Zheng ZZ, Pang SY, Li JJ. Numerical and experimental investigation of the thermal behavior and microstructure of wire arc additive manufactured 316L stainless steel straight wall part. IOP Conf Ser Mater Sci Eng 2022;1270:012084. https://doi.org/10.1088/1757-899x/1270/1/012084.

[25] Montevecchi F, Venturini G, Scippa A, Campatelli G. Finite Element Modelling of Wire-arc-additive-manufacturing Process. Procedia CIRP, vol. 55, Elsevier B.V.; 2016, p. 109–14. https://doi.org/10.1016/j.procir.2016.08.024.

[26] Ufot E, Lebele-Alawa BT, Bob-Manuel KDH. Influence of Convection Heat Transfer Coefficient on Heat Transfers and Wall Temperatures of Gas-turbine Combustors. vol. 1. 2011.

[27] Halisch C, Radel T, Tyralla D, Seefeld T. Measuring the melt pool size in a wire arc additive manufacturing process using a high dynamic range two-colored pyrometric camera. Welding in the World 2020;64:1349–56. https://doi.org/10.1007/s40194-020-00892-5.

[28] Sun J, Hensel J, Köhler M, Dilger K. Residual stress in wire and arc additively manufactured aluminum components. J Manuf Process 2021;65:97–111. https://doi.org/10.1016/j.jmapro.2021.02.021.

[29] Rodrigues TA, Duarte V, Miranda RM, Santos TG, Oliveira JP. Current status and perspectives on wire and arc additive manufacturing (WAAM). Materials 2019;12. https://doi.org/10.3390/ma12071121.

[30] Grilli N, Hu D, Yushu D, Chen F, Yan W. Crystal plasticity model of residual stress in additive manufacturing 2021.

[31] Wu B, Pan Z, Ding D, Cuiuri D, Li H, Xu J, et al. A review of the wire arc additive manufacturing of metals: properties, defects and quality improvement. J Manuf Process 2018;35:127–39. https://doi.org/10.1016/j.jmapro.2018.08.001.

[32] Williams SW, Martina F, Addison AC, Ding J, Pardal G, Colegrove P. Wire + Arc additive manufacturing. Materials Science and Technology (United Kingdom) 2016;32:641–7. https://doi.org/10.1179/1743284715Y.0000000073.

[33] Yang J, Wang A. Microstructure Evolution and Performance of AA2024 Alloy Through Wire-Arc Additive Manufacturing Under Different Heat Inputs. Metals (Basel) 2024;14. https://doi.org/10.3390/met14111265.

[34] Sarıkaya M, Başcıl Önler D, Dağlı S, Hartomacıoğlu S, Günay M, Królczyk GM. A review on aluminum alloys produced by wire arc additive manufacturing (WAAM): Applications, benefits, challenges and future trends. Journal of Materials Research and Technology 2024;33:5643–70. https://doi.org/10.1016/j.jmrt.2024.10.212.

[35] S. Elangovan, M. Jayaram, Saravan M, Hari Ganesh, Subash P. Wire Arc Additive Manufacturing of Aluminium Alloys using GTAW - A Review, European Alliance for Innovation n.o.; 2024. https://doi.org/10.4108/eai.23-2-2024.2346993.